J. Fluid Mech. (2014), *vol.* 752, *pp.* 462–484.
doi:10.1017/jfm.2014.346

A class of exact Navier–Stokes solutions for homogeneous flat-plate boundary layers and their linear stability

Michael O. John†, Dominik Obrist and Leonhard Kleiser

Institute of Fluid Dynamics, ETH Zurich, CH-8092 Zurich, Switzerland

(Received 19 December 2013; revised 5 May 2014; accepted 14 June 2014;
first published online 7 July 2014)

We introduce a new boundary layer formalism on the basis of which a class of exact solutions to the Navier–Stokes equations is derived. These solutions describe laminar boundary layer flows past a flat plate under the assumption of one homogeneous direction, such as the classical swept Hiemenz boundary layer (SHBL), the asymptotic suction boundary layer (ASBL) and the oblique impingement boundary layer. The linear stability of these new solutions is investigated, uncovering new results for the SHBL and the ASBL. Previously, each of these flows had been described with its own formalism and coordinate system, such that the solutions could not be transformed into each other. Using a new compound formalism, we are able to show that the ASBL is the physical limit of the SHBL with wall suction when the chordwise velocity component vanishes while the homogeneous sweep velocity is maintained. A corresponding non-dimensionalization is proposed, which allows conversion of the new Reynolds number definition to the classical ones. Linear stability analysis for the new class of solutions reveals a compound neutral surface which contains the classical neutral curves of the SHBL and the ASBL. It is shown that the linearly most unstable Görtler–Hämmerlin modes of the SHBL smoothly transform into Tollmien–Schlichting modes as the chordwise velocity vanishes. These results are useful for transition prediction of the attachment-line instability, especially concerning the use of suction to stabilize boundary layers of swept-wing aircraft.

Key words: boundary layer stability, boundary layers, Navier–Stokes equations

1. Introduction

Exact solutions to the Navier–Stokes equations (NSE) are useful for drawing conclusions about fundamental properties of flow fields, for validating numerical simulations and for supporting experimental investigations. Because no straightforward method for deriving them exists, new solutions were often formulated without any connection to similar known solutions (Drazin & Riley 2006), and sometimes identical solutions have been derived independently a number of times. In the first part of the present work, we combine several known exact solutions for boundary layer flows

† Email address for correspondence: john@ifd.mavt.ethz.ch

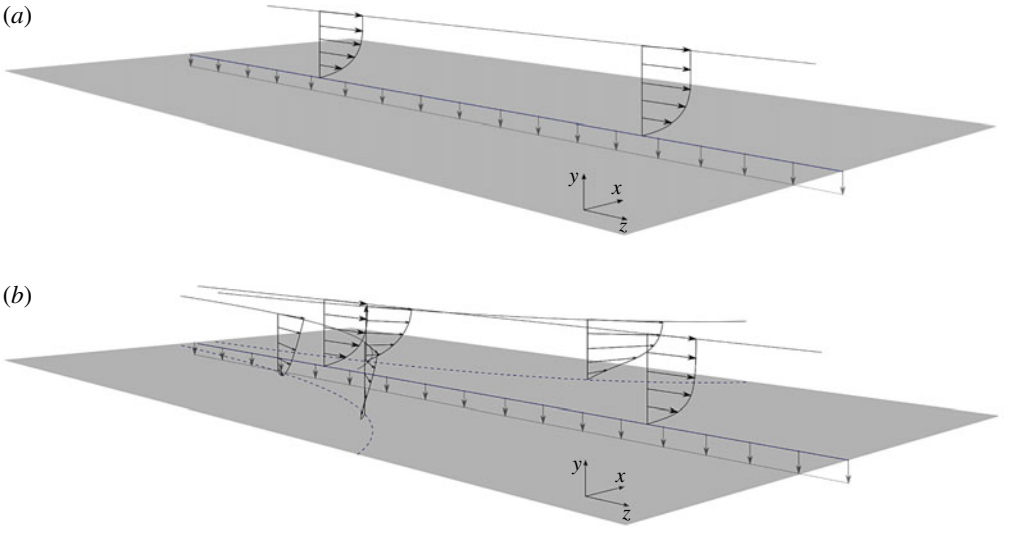

FIGURE 1. Sketch of (*a*) the ASBL flow and (*b*) the SHBL flow, along with the coordinate system. The dashed lines show wall skin friction lines.

into a single solution by introducing a new definition of the boundary layer similarity variable. In the second part, the linear stability of the new, compound solution is analysed, unveiling new findings for the stability of the classical, known solutions.

We study the incompressible laminar flow past a flat plate with one homogeneous direction. A variety of seemingly unrelated solutions exists in this setting, for example the plane stagnation (Hiemenz) boundary layer (HBL, Hiemenz 1911), where the axis of homogeneity z is perpendicular to the plane of the flow (x, y), or the two-dimensional asymptotic suction boundary layer (ASBL, Preston 1948) depicted in figure 1(*a*), where the axis of homogeneity z is parallel to the plane of the flow (y, z). Later it was realized that both belong to the class of Falkner–Skan (FS) boundary layers (Rosenhead 1963). Still, to date their stability properties have not been investigated in a common framework. Additionally, various modifications of the HBL exist, such as the three-dimensional swept Hiemenz boundary layer (SHBL), which belongs to the class of Falkner–Skan–Cooke (FSC) boundary layers (Cooke 1950). The SHBL is depicted in figure 1(*b*), with wall-normal coordinate y, chordwise direction x and homogeneous sweep direction z. It serves as a model for the attachment-line flow of swept-wing configurations (Pfenninger 1965; Gaster 1967; Poll 1979).

Another closely related boundary layer is the oblique impingement boundary layer (OIBL), which is found when the direction of impingement is tilted by an angle of attack within the plane of the HBL flow, as has been derived independently by Stuart (1959), Tamada (1979) and Dorrepaal (1986). Minor differences in the governing equations due to different choices of the pressure gradients have been clarified by Drazin & Riley (2006) and Tooke & Blyth (2008). Finally, even more adaptations have been realized, e.g. time-varying stagnation flow by Kolomenskiy & Moffatt (2012) and stretching walls by Lok, Amin & Pop (2006). Porous boundaries may easily be accounted for by allowing for a wall-normal suction velocity (Wang 1991).

Despite their variety, two common features of all the above flows are the presence of a flat plate and a homogeneous direction z parallel to the plate, along which the

boundary layer thickness remains constant. In this work, we present a compound formalism that unifies these solutions (ASBL, SHBL and OIBL). It has already been briefly introduced in John, Obrist & Kleiser (2012), and we extend it in the present paper. In the first part of this work, concerning the exact solution, there are two main findings: first, the physically sensible limit of a SHBL with vanishing chordwise velocity u is the ASBL, provided there is wall suction (see figure 1); second, an exact solution is presented which may depend explicitly on both an angle of attack and a sweep angle. This gives rise to the swept OIBL, a combination of the classical SHBL and OIBL, which serves as an exact Navier–Stokes solution describing the flow close to the leading edge of an airplane wing with or without wall suction and under any angle of attack or any angle of sweep, including the limits 0 and $\pi/2$.

The second part of this work consists of a linear stability investigation of the new class of solutions. The stability of the particular class of solutions presented here gives further insight into the attachment-line instability (Pfenninger 1965; Gaster 1967; Poll 1979; Saric, Reed & White 2003) found on swept airplane wings. This subcritical instability, which may cause turbulence immediately downstream of the leading edge, occurs independently of the classical Tollmien–Schlichting (TS) and cross-flow bypass transition scenarios (Owen & Randall 1952; Saric *et al.* 2003). Understanding the transition processes of this boundary layer at the leading-edge of a swept wing is a crucial step towards delaying or inhibiting the onset of turbulence along the wing, and thus towards a reduction of airplane drag and fuel consumption (Arnal *et al.* 1997). As yet, these processes are not fully understood and attempts to explain the transition comprise elaborate linear biglobal stability analyses (Theofilis *et al.* 2003; Robitaillié-Montané 2005) and numerical simulations of secondary instability phenomena (Obrist, Henniger & Kleiser 2012). Therefore, the combination of the linear stability results of all of the above classical solutions and the presentation of a compound neutral surface appears useful.

In the case of the ASBL, the critical Reynolds number of the TS mode is $Re^{AS}_{class,\,crit} \approx 54\,370$ (Hocking 1975), and large portions of the neutral curve have been reported by Herron, Von Kerczek & Tozzi (1985). For the SHBL, the instability mode is named after Görtler (1955) and Hämmerlin (1955) (GH), and the critical Reynolds number is $Re^{SH}_{crit} \approx 583.1$; this was determined experimentally by Poll (1979) and by means of stability theory by Hall, Malik & Poll (1984), who also included wall suction in their analysis. Extensions of the GH mode to higher-order chordwise ansatz functions have been carried out by Obrist & Schmid (2003) and Theofilis *et al.* (2003), who confirmed the results for the critical values of Hall *et al.* (1984).

With our new compound solution formalism, it is possible to analyse the stability of the SHBL and the ASBL in a unified framework as a function of a single Reynolds number and wavenumber. Our results provide a smooth neutral surface which contains the results for the SHBL and the ASBL. In particular, both the three-dimensional GH and the two-dimensional TS modes are shown to be parametric variations of the same linear instability. They merge smoothly when the base flow is varied from a three-dimensional to a two-dimensional one.

The remainder of this paper is structured as follows. In § 2 the governing equations of the classical and new boundary layer formalisms are introduced. A non-dimensionalization for the new class of solutions is presented in § 3. The linear stability analysis of these solutions is carried out in § 4. Section 5 concludes the paper.

2. Derivation of the new set of compound boundary layer solutions

2.1. *The classical similarity solutions*

2.1.1. *The SHBL*

The new formalism is inspired by the three-dimensional swept stagnation flow illustrated in figure 1(*b*), which is obtained from superposition of a plane stagnation flow (Hiemenz 1911) and a uniform sweep velocity. Using the assumption of a swept plate of infinite extent ($\partial/\partial z = 0$), the classical SHBL formalism (e.g. Schlichting 1979, p. 95) reads

$$U(x, y) = ax, \quad V(x, y) = -ay, \quad W(x, y) = W_\infty, \tag{2.1a}$$

$$\eta^{SH} := \sqrt{a/\nu} \cdot y, \tag{2.1b}$$

$$u(x, \eta) = axf'(\eta), \quad v(\eta) = -\sqrt{a\nu} f(\eta), \quad w(\eta) := W_\infty g(\eta), \tag{2.1c}$$

where u, v and w are the velocity components in the x, y and z directions, respectively, with capital letters referring to the outer velocity field and lowercase letters to the full velocity field, a is a strain rate and W_∞ is a wall-parallel far-field velocity component. The self-similar functions f and g are determined from the set of ordinary differential equations (ODEs)

$$f''' + ff'' - f'^2 + 1 = 0, \tag{2.2a}$$

$$g'' + fg' = 0 \tag{2.2b}$$

(Hiemenz 1911), subject to the boundary conditions

$$f(0) = \kappa^{SH}, \quad f'(0) = 0, \quad f'(\infty) = 1, \tag{2.3a}$$

$$g(0) = 0, \quad g(\infty) = 1, \tag{2.3b}$$

which allow for the wall-normal suction velocity $-V_0$ at the wall,

$$\kappa^{SH} = V_0/\sqrt{\nu a}. \tag{2.4}$$

The non-dimensionalization associated with this ansatz is based on the reference velocity W_∞ and the reference length scale $\Delta^{SH} = \sqrt{\nu/a}$, listed in table 1. The superscript $(\cdot)^{SH}$ is used to mark quantities which depend on this non-dimensionalization. Owing to the self-similarity of the flow, the strain rate a may be expressed in terms of two arbitrary (dependent) parameters as $a = U_l^{SH}/l^{SH}$, where U_l^{SH} is a velocity scale in the x direction and l^{SH} is a length scale related to the y direction. This will be of importance for the comparison with the ASBL and for the derivation of a new formalism.

2.1.2. *The ASBL*

The ASBL, which also satisfies the condition $\partial/\partial z = 0$, is depicted in figure 1(*a*) and given by $w(y) = W_\infty[1 - \exp(-yV_0/\nu)]$, $v = -V_0$ (e.g. Preston 1948). Here, we also formally express it as a FS boundary layer (Rosenhead 1963) with z as the streamwise direction, using the following (arbitrary) representation of the streamwise velocity W_∞ as a function of a length scale l^{AS} and a strain rate γ^{AS}:

$$W_\infty = \gamma^{AS} \cdot l^{AS}. \tag{2.5}$$

Formalism	U_{ref}	Δ	Re	κ
$(\cdot)^{SH}$, (2.1)	W_∞	$\sqrt{\nu/a}$	$W_\infty/\sqrt{\nu a}$	$V_0/\sqrt{\nu a}$
$(\cdot)^{AS}$, (2.6)	W_∞	$\sqrt{\nu/\gamma}$	$W_\infty/\sqrt{\nu\gamma}$	$V_0/\sqrt{\nu\gamma}$
Compound, (2.12)	Q_l	$\sqrt{\nu/\gamma}$	$Q_l/\sqrt{\nu\gamma}$	$V_0/\sqrt{\nu\gamma}$

TABLE 1. Reference quantities U_{ref} and Δ used for non-dimensionalization, along with the resulting Reynolds number Re and dimensionless suction κ for the three different formalisms.

This allows us (see Rosenhead 1963, p. 245) to write the ASBL as

$$U(x,y)=0, \quad V(x,y)=-V_0, \quad W(x,y)=W_\infty, \tag{2.6a}$$

$$\eta^{AS} := \sqrt{\gamma^{AS}/\nu}\cdot y, \tag{2.6b}$$

$$u(\eta)=0, \quad v(\eta)=-\sqrt{\gamma^{AS}\nu}\cdot\kappa^{AS}, \quad w(\eta):=W_\infty g(\eta), \tag{2.6c}$$

where the non-dimensional suction is expressed as $\kappa^{AS}=V_0/\sqrt{\nu\gamma^{AS}}$. Again, a superscript $(\cdot)^{AS}$ is introduced to indicate those quantities which depend on this non-dimensionalization. The self-similar function g is determined from the ODE

$$g''+\kappa^{AS}g'=0, \tag{2.7a}$$

$$g(0)=0, \quad g(\infty)=1. \tag{2.7b}$$

The Reynolds number associated with the formalism (2.6) is listed in table 1. It is based on a non-dimensionalization with the standard reference velocity W_∞ and the non-standard reference length scale $\Delta^{AS}=\sqrt{\nu/\gamma^{AS}}$. The more familiar classical Reynolds number $Re^{AS}_{class}=W_\infty/V_0$ is obtained for the particular choice of $l^{AS}=l^{AS}_{class}\equiv W_\infty\nu/V_0^2$, which leads to $\Delta^{AS}_{class}=\nu/V_0$. This is, however, not the only admissible choice. Later, a different value for l^{AS} will be chosen in order to define a Reynolds number which may be transformed smoothly to the Reynolds number of the new formalism.

2.1.3. *Singularity of the swept Hiemenz formalism*

The motivation for our derivation of a new class of solutions is the fact that the SHBL formalism (2.1) becomes singular in a limiting case which is nevertheless physically meaningful. Whereas (2.1) describes a three-dimensional flow generated by two independent far-field velocities (W_∞ and $U_l^{SH}=a\cdot l^{SH}$), the similarity coordinate η^{SH} depends only on the velocity component U_l^{SH}; see (2.1*b*). Therefore, this formalism only allows for the two-dimensional parametric limit of no sweep ($W_\infty=0$), for which it describes the HBL. It becomes singular in the parametric limit of full sweep where $a\to 0$ and $U_l^{SH}\to 0$, because then $\eta^{SH}\to 0$. Nevertheless, we will show in the next section that this full-sweep limit is sensible because it is described by the ASBL, (2.6), which is the homogeneous flow in the z direction past a flat plate, in the absence of any flow in the x direction, for wall suction $\kappa^{SH}>0$.

The fact that the two flow configurations are so closely related physically but are treated so differently mathematically (with different rescaled coordinates η^{SH} and η^{AS} and different ansatz functions f and g) is a limitation which we will overcome by introducing a new compound formalism in the next subsection.

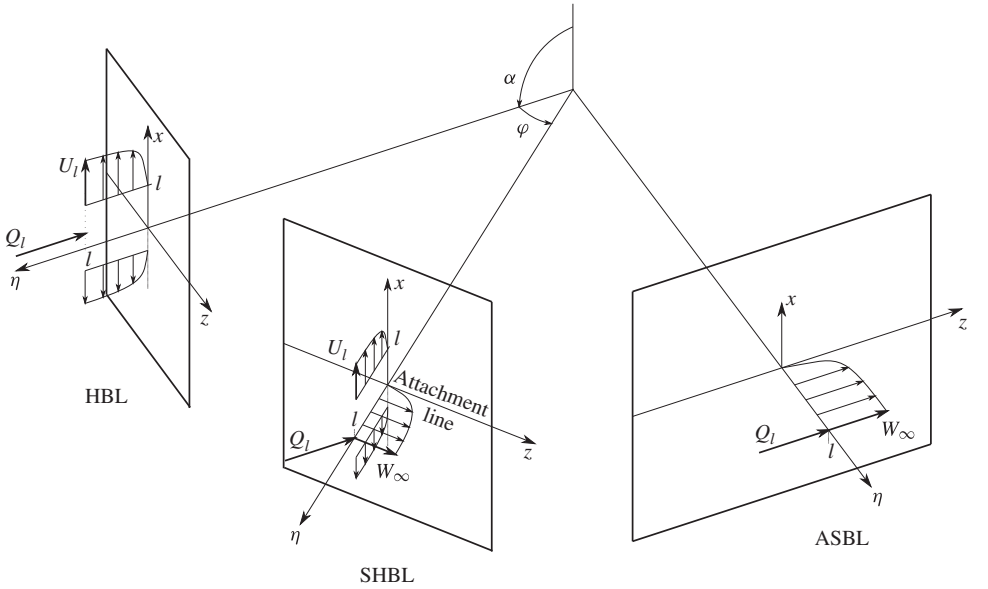

FIGURE 2. Flow fields for three different angles φ, displaying Q_l, φ, U_l, W_∞ and l (with $\alpha = \pi/2$).

2.2. *Compound boundary layer formalism*

First, we describe the far-field flow; then we present the inner boundary layer flow and, finally, take the formal parametric limits to recover the classical solutions.

2.2.1. *Far-field flow*

The steady far field for the three velocity components $\{U, V, W\}$ and pressure P at constant density ρ (figure 2) consists of an impingement component ($\gamma \cos\varphi \sin\alpha$) and a chordwise shear component ($\gamma \cos\alpha$):

$$U(x, y) = (x \sin\alpha \cos\varphi + y \cos\alpha) \cdot \gamma + U_0, \tag{2.8a}$$

$$V(x, y) = -y \sin\alpha \cos\varphi \cdot \gamma, \tag{2.8b}$$

$$W(x, y) := W_\infty, \tag{2.8c}$$

$$(1/\rho) \cdot (P_0 - P(x, y)) = (x^2 + y^2)/2 \cdot \gamma^2 \sin^2\alpha \cos^2\varphi + U_0 \gamma x \sin\alpha \cos\varphi, \tag{2.8d}$$

where α is the impingement angle in the (x, y)-plane (i.e. the complement of the angle of attack, $\pi/2 - \alpha$), φ is the sweep angle of the infinite plate in the (y, z)-plane, P_0 denotes the reference pressure and U_0 is some constant additional shear flow in the chordwise x direction. The pressure equation is explicitly included in the analysis because its implicit treatment in different ways by previous authors (Stuart 1959; Tamada 1979; Dorrepaal 1986) has caused confusion, which was later clarified by Drazin & Riley (2006). The angle φ is spanned by the far-field velocity components in the sweep direction (W_∞) and the x direction (U_l^{SH}), taken at some height l above the plane:

$$\tan\varphi = W_\infty / U_l^{SH}. \tag{2.9}$$

Analogously to §§ 2.1.1 and 2.1.2, the global far-field velocity magnitude

$$Q_l \equiv \sqrt{(U_l^{SH})^2 + W_\infty^2} \tag{2.10}$$

at height l above the plate (figure 2) may be represented by a length scale l and a strain rate γ in the direction of the free stream according to

$$Q_l = \gamma \cdot l. \tag{2.11}$$

This representation renders Q_l a generalized velocity and γ a generalized strain rate, which are not necessarily oriented in the x and z directions. Rather, Q_l impinges on the plate at an angle φ measured in a plane parallel to the wall at distance l above the plate (figure 2). The relation between γ and a, used for the SHBL formalism (2.1), is $a \equiv \gamma \cos\varphi$. The non-dimensionalization of the NSE used for the present formulation takes Q_l as the reference velocity and $\Delta = \sqrt{\nu/\gamma}$ as the reference length scale for calculating the Reynolds number (table 1). The absence of a superscript indicates quantities for the new, compound formalism.

2.2.2. *The boundary layer*

The full velocity field satisfies the boundary conditions at the wall and matches the far-field flow. It is found by introducing the compound formalism for the near-field solution $\{u, v, w, p\}$, based on a rescaling of η:

$$\eta := \sqrt{Q_l/(\nu l)} \cdot y = \sqrt{\gamma/\nu} \cdot y, \tag{2.12a}$$

$$u(x, \eta) = \gamma x f'(\eta) + \sqrt{\gamma\nu} h(\eta), \tag{2.12b}$$

$$v(\eta) = -\sqrt{\gamma\nu} f(\eta), \tag{2.12c}$$

$$w(\eta) := Q_l \sin\varphi g(\eta), \tag{2.12d}$$

$$p(x, \eta) := -\frac{\rho}{2}[\gamma^2 \cos^2\varphi \sin^2\alpha (x^2 + 2x \cdot C) + 2\nu\gamma (f^2/2 + f')] + p_0, \tag{2.12e}$$

where p_0 is some reference pressure, h is a function describing the shear flow in the x direction, with $H'(\eta) = h(\eta)$, and C is some constant. The solutions to the formalism, f, g and h, are obtained from the ODEs

$$f''' + f f'' - f'^2 + \cos^2\varphi \sin^2\alpha = 0, \tag{2.13a}$$

$$h'' + f h' - f' h = \text{const.}, \tag{2.13b}$$

$$g'' + f g' = 0. \tag{2.13c}$$

The boundary conditions are

$$f(0) = \kappa, \quad f'(0) = 0, \quad f'(\infty) = \cos\varphi \sin\alpha, \tag{2.14a}$$

$$g(0) = 0, \quad g(\infty) = 1, \tag{2.14b}$$

$$h(0) = 0, \quad h'(\infty) = \cos\alpha, \tag{2.14c}$$

where $\kappa := V_0/\sqrt{\nu\gamma}$ is the dimensionless wall-normal velocity at the wall, such that $v(0) = -V_0$.

The solutions to these equations depend on the three parameters α, φ and κ, which provide the necessary additional degree of freedom to explore the whole range of solutions from the HBL ($\varphi = 0$, $\alpha = \pi/2$) via the SHBL ($0 < \varphi < \pi/2$, $\alpha = \pi/2$) to the ASBL ($\varphi = \pi/2$, $\alpha = \pi/2$). Also, the OIBL ($\varphi = 0$, $0 < \alpha < \pi/2$) and swept OIBL ($0 < \varphi < \pi/2$, $0 < \alpha < \pi/2$) are described by (2.13). A summary of the parameter space of the solutions to (2.13) is given in table 2, and a graphical representation can be found in figure 3.

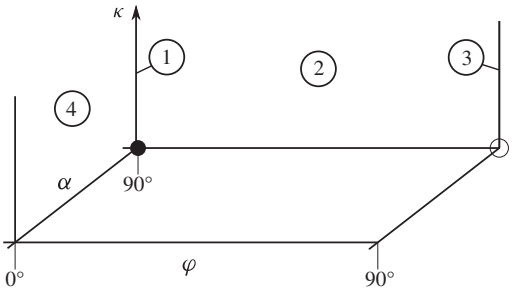

FIGURE 3. Schematic of the parameter space (angle of impingement α, sweep angle of the flat plate φ, wall suction κ) and location of the cases 1–4 in table 2. The filled circle represents the classical plane HBL, and the open circle represents the location of the Blasius boundary layer (not contained in (2.15)).

Boundary layer flow	α	φ
The general case	$(0, \pi/2]$	$[0, \pi/2]$
1. (Suction) Hiemenz/plane stagnation	$\pi/2$	0
2. (Suction) swept Hiemenz/swept stagnation	$\pi/2$	$[0, \pi/2)$
3. Asymptotic suction	$\pi/2$	$\pi/2$
4. (Suction) oblique impingement	$(0, \pi/2]$	0

TABLE 2. The parameter ranges for (2.13) in the general case and in the classical limits.

At this point it is of interest to compare the present scaling (2.12*a*) of the wall-normal coordinate η with other formalisms from the literature. While there are various ways of obtaining exact solutions to stagnation flows, they are all limited by at least one restriction that does not apply here. The class of two-dimensional FS boundary layers, as discussed by Schlichting (1979) and Rosenhead (1963), is distinctly different because it inherently depends on only one velocity component. Even if the flows are extended to three-dimensional FSC boundary layers, the one-dimensional scaling of the similarity coordinate η remains (as shown above for the SHBL). Other approaches to describing three-dimensional stagnation flow solutions fall into two categories. One group assumes axisymmetry (e.g. Rosenhead 1963, p. 417). Schlichting (1979, p. 100) even refers to the three-dimensional case as 'the' axisymmetrical case. This assumption clearly contradicts the homogeneity assumption, $\partial/\partial z = 0$, made here. The other group of solutions obtain their three-dimensionality through two independent ansatz functions for the chordwise and streamwise velocity components, which are both linked to the wall-normal component (e.g. Howarth 1951; Wang 1991; Weidman 2012). These flows obtain their three-dimensionality from a quasi-axisymmetric flow where the chordwise and streamwise axes are merely rescaled in different ways. However, they do not overcome the singularity discussed above either. In summary, to the best of our knowledge, so far there is no other three-dimensional boundary layer formalism which allows for a homogeneous direction and which contains both of the limiting cases found when either one of the independent velocity components U_l^{SH} and W_∞ vanishes.

2.2.3. *Recovering the classical limits*

Here it is very briefly shown that the formalism (2.12) contains the classical boundary layers as parametric limits of the parameter space $\{\varphi, \kappa, \alpha\}$. First, normal impingement ($\alpha = \pi/2$) is considered, for which no sweep ($\varphi = 0$ in (2.13)) recovers the HBL of (2.2). At the same time, $W_\infty \equiv Q_l \sin\varphi = 0$ and $\gamma = a$, so that η of (2.12*a*) becomes η^{SH} of (2.1*b*).

The SHBL is obtained for $0 < \varphi < \pi/2$, in which case the governing equations, the boundary conditions and all non-dimensional parameters change according to the rescaling (see table 1), which is discussed in more detail alongside the physical scaling presented in § 3.2.

The full-sweep situation recovers the ASBL by setting $\varphi = \pi/2$ in (2.13*a*) to obtain $f = \text{const.} = \kappa$ from (2.14*a*). Substituting this into (2.13*c*) recovers (2.7*a*). At the same time, $U_l^{SH} \equiv Q_l \cos\varphi = 0$, and η of (2.12*a*) becomes η^{AS} of (2.6*b*).

Oblique impingement is obtained upon inserting $\varphi = 0$ and $0 < \alpha < \pi/2$ into (2.13), which reduces (2.13) to the classical OIBL, where η depends only on $U_l^{SH} \equiv Q_l \cos\varphi = Q_l$. For brevity, these steps are not repeated here and the reader is referred to the works of Stuart (1959), Tamada (1979) and Dorrepaal (1986) for details.

In the remainder of this paper we omit non-zero angles of attack and restrict ourselves to the case of $\alpha = \pi/2$. This leads to the simplified set of equations

$$f''' + ff'' - f'^2 + \cos^2\varphi = 0, \tag{2.15a}$$

$$g'' + fg' = 0, \tag{2.15b}$$

$$f(0) = \kappa, \quad f'(0) = 0, \quad f'(\infty) = \cos\varphi, \tag{2.15c}$$

$$g(0) = 0, \quad g(\infty) = 1. \tag{2.15d}$$

This covers the boundary layers depicted in figure 2, for which some example solutions are shown in figure 4. At this point, transformations between the Reynolds numbers and non-dimensional wall-suction velocities of the three formalisms (2.1), (2.6) and (2.12) may already be formulated, as the reference velocities and reference length scales have been defined (see table 1):

$$\frac{Re^{SH}}{Re|_{\kappa=0}} = \frac{W_\infty}{Q_l}\sqrt{\frac{\gamma|_{\kappa=0}}{a}} = \frac{\sin\varphi}{\sqrt{\cos\varphi}}, \tag{2.16}$$

$$\frac{Re^{AS}}{Re|_{\varphi=\pi/2}} = \frac{W_\infty}{Q_l|_{\varphi=\pi/2}} = 1, \tag{2.17}$$

$$\frac{\kappa^{SH}}{\kappa} = \sqrt{\frac{\gamma}{a}} = \frac{1}{\sqrt{\cos\varphi}}, \tag{2.18}$$

$$\frac{\kappa^{AS}}{\kappa} = 1. \tag{2.19}$$

Note that the classical Reynolds number Re^{SH} does not depend on κ and that Re^{AS} is independent of φ. Furthermore, the transformation (2.16) illustrates that $Re^{SH} \to \infty$ in the full-sweep limit ($\varphi \to 90°$) when a vanishes, even if W_∞ remains finite.

3. Physical scaling

This section aims to provide precise physical meaning to the quantities, such as l or φ, introduced during the derivation of the compound formalism in § 2.2. While the

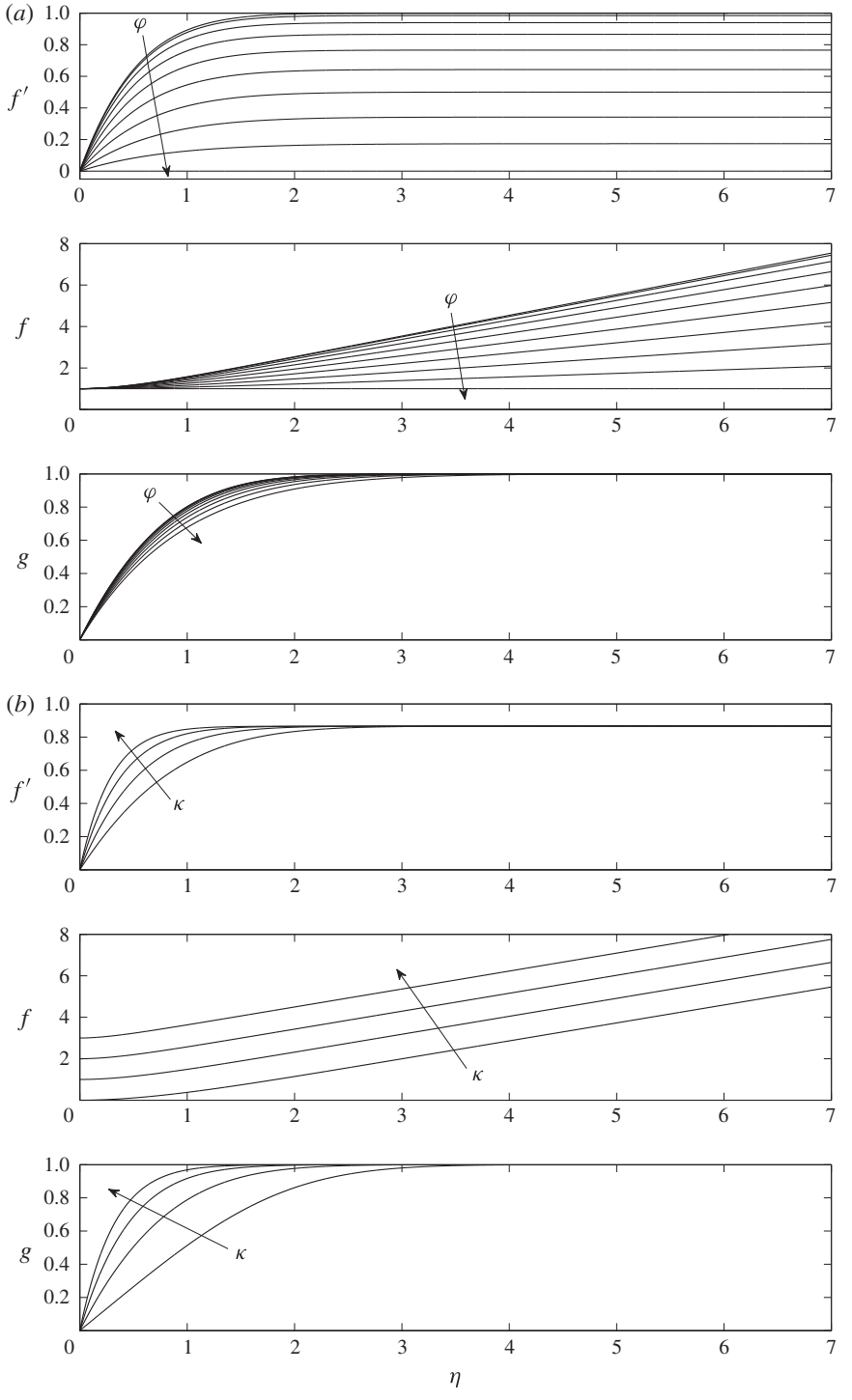

FIGURE 4. Example solutions of (2.15) at (*a*) constant suction $\kappa = 1$ for sweep angles $\varphi = \{0°, 10°, \ldots, 90°\}$ and (*b*) constant angle $\varphi = 30°$ for suction values $\kappa = \{0, 1, 2, 3\}$.

mathematical solution is complete at this point, a sound non-dimensionalization and physical scaling using the reference velocity U_{ref} and length scale Δ for (2.15) are indispensable for practical applications, as well as for the stability theory of § 4.

This section is structured as follows. First, we choose a length scale l in § 3.1, which allows explicit computation of the reference quantities and the Reynolds number in § 3.2. For this choice of l, explicit transformations to the classical Reynolds numbers are presented in § 3.3.

3.1. *Choice of the length scale l*

One admissible choice for the length scale l is the dimensional boundary layer momentum thickness θ of the w velocity component in the z direction. The physical momentum thickness θ and its non-dimensional counterpart $\bar{\theta}$ are, by definition, related by the reference length scale Δ, which itself depends on the non-dimensionalization (table 1):

$$\bar{\theta}(\varphi, \kappa) \cdot \Delta \equiv \theta(\varphi, \kappa). \tag{3.1}$$

The dependence of $\bar{\theta}$ on φ and κ is easily seen from its definition,

$$\bar{\theta}(\varphi, \kappa) := \int_0^\infty g(\varphi, \kappa)(1 - g(\varphi, \kappa))\, \mathrm{d}\eta. \tag{3.2}$$

The choice $l = \theta$ is beneficial for the following two reasons. First, it is measured in the wall-normal direction, in which all solutions of (2.15) have a non-zero velocity component, so that l never vanishes. It is bounded in the entire parameter space (φ, κ), because it is a function of both the wall suction and the strain of the far field due to stagnation flow. In contrast, $l^{SH} = U^{SH}/a$ of the classical SHBL formalism simultaneously measures a distance in the x and y directions; so, for vanishing U_l^{SH}, the classical length scale l^{SH} becomes undefined. Second, the choice $l = \theta$ is advantageous because θ does not explicitly depend on only one of the physical parameters (a or V_0). Rather, it depends on the solution to the NSE. Naturally, this invokes a dependence on the Reynolds number itself and incorporates the influence of the far field and of the boundary conditions into a single length scale. Lew (1956) already stated that the most significant Reynolds number for flows over a porous cylinder 'appears to be composed of the magnitude of the suction velocity at the wall and the radius of the cylinder'. Therefore, the dependence of Re on θ, which depends implicitly on both the strain rate a and the suction V_0, is consistent with Lew's statement.

3.2. *New Reynolds number as a function of φ and κ*

With $l = \theta(\varphi, \kappa)$, the value of $\bar{\theta}$ can be determined as a function of φ and κ. We exploit the fact that θ is related to $\bar{\theta}$ through (3.1) and use the definition of γ in (2.11) to obtain

$$\bar{\theta}(\varphi, \kappa) = \frac{\theta}{\Delta} = \frac{\theta\sqrt{\gamma}}{\sqrt{\nu}} = \frac{\theta\sqrt{Q_l}}{\sqrt{\theta\nu}} = \sqrt{\frac{Q_l\theta}{\nu}} = \frac{Q_l}{\sqrt{\gamma\nu}} = Re(\varphi, \kappa). \tag{3.3}$$

The Reynolds number Re of the compound formalism (2.12) is thus identical to the non-dimensional boundary layer thickness $\bar{\theta}$. This is due to the self-similarity of the governing equations (2.15) and the choice of $l = \theta$.

While one could obtain an impression of Re by simply solving (3.2) numerically for various values of φ and κ, the dependencies along the axes $\kappa = 0$ and $\varphi = \pi/2$ may also be derived analytically as follows. Integration of (3.2) at the point $\{\varphi = 0, \kappa = 0\}$ results in

$$\bar{\theta}_0 := \bar{\theta}(\varphi = 0, \kappa = 0) = \int_0^\infty g(0,0)(1 - g(0,0))\,\mathrm{d}\eta \approx 0.4042, \tag{3.4}$$

which is the non-dimensional momentum thickness of the HBL (Rosenhead 1963, p. 471). An expression for $Re(\varphi)|_{\kappa=0}$ may also be found analytically by using the non-dimensional thickness $\bar{\theta}^{SH}$ of the classical formalism (2.1):

$$Re(\varphi)|_{\kappa=0} = \bar{\theta}(\varphi)_{\kappa=0} = \frac{\theta(\varphi, \kappa = 0)}{\Delta(\varphi, \kappa = 0)} = \frac{\bar{\theta}^{SH}\Delta^{SH}}{\Delta(\varphi, \kappa = 0)} = \frac{\bar{\theta}_0}{\sqrt{\cos\varphi}}. \tag{3.5a}$$

The first equality is (3.3), the second is (3.1), and the third holds because θ of the SHBL is the product of $\bar{\theta}^{SH}$ and the length scale Δ^{SH} of the classical formalism. The classical result is $\bar{\theta}^{SH} \equiv \bar{\theta}_0 \approx 0.4042$, which is known from the literature for (2.2). Finally, Δ^{SH}/Δ is evaluated from table 1.

Following the same reasoning, $Re(\kappa)|_{\varphi=\pi/2}$ is obtained from

$$Re(\kappa)|_{\varphi=\pi/2} = \bar{\theta}(\kappa)_{\varphi=\pi/2} = \frac{\theta\left(\varphi = \dfrac{\pi}{2}, \kappa\right)}{\Delta\left(\varphi = \dfrac{\pi}{2}, \kappa\right)} = \frac{\nu}{2V_0}\sqrt{\frac{\gamma}{\nu}} = \frac{\sqrt{\nu\gamma}}{2V_0} = \frac{1}{2\kappa}, \tag{3.5b}$$

where the momentum thickness of the ASBL, $\theta(\varphi = \pi/2, \kappa) = \nu/(2V_0)$, has been used.

A contour plot of $Re(\varphi, \kappa)$ is obtained by numerically solving (3.2) with shooting integration (figure 5) and summarizes (3.2)–(3.5). It is interesting to see that Re is bounded within the entire parameter space depicted in figure 3, except for the singular limit of the Blasius boundary layer, $\{\alpha = \pi/2, \varphi \to 90°, \kappa \to 0\}$.

3.3. *Transformation to the classical Reynolds numbers Re^{SH} and Re^{AS}*

The Reynolds number Re, which has been computed for the entire (φ, κ) parameter space, may be transformed explicitly to the classical definitions Re^{SH} and Re^{AS} (see table 1) by employing the transformations (2.16) and (2.17) together with (3.5):

$$Re^{SH} = \frac{\sin\varphi}{\sqrt{\cos\varphi}} \cdot \frac{\bar{\theta}_0}{\sqrt{\cos\varphi}} = \bar{\theta}_0 \cdot \tan\varphi, \tag{3.6a}$$

$$Re^{AS} = 1/(2\kappa). \tag{3.6b}$$

A SHBL with suction, described by $\{Re^{SH}, \kappa^{SH}\}$, may be transformed to the new parameters by obtaining φ from (3.6*a*) and then $\kappa = \kappa^{SH}\sqrt{\cos\varphi}$ from (2.18). Likewise, an ASBL, described by Re^{AS}, may be converted to κ by (3.6*b*).

The fact that the classical Reynolds number Re^{SH} depends only on the single parameter φ, as seen in (3.6*a*), may easily be verified by dimensional analysis: the parameters $\{W_\infty, \nu, a\}$ can form exactly one independent non-dimensional quantity, but no independent reference length scale is provided. By construction, the angle φ relates W_∞ and a in (2.9) via the auxiliary variable $l^{SH} = U^{SH}/a$. Meanwhile, because no independent length scale exists, l^{SH} must itself be constructed using ν. Thus, the

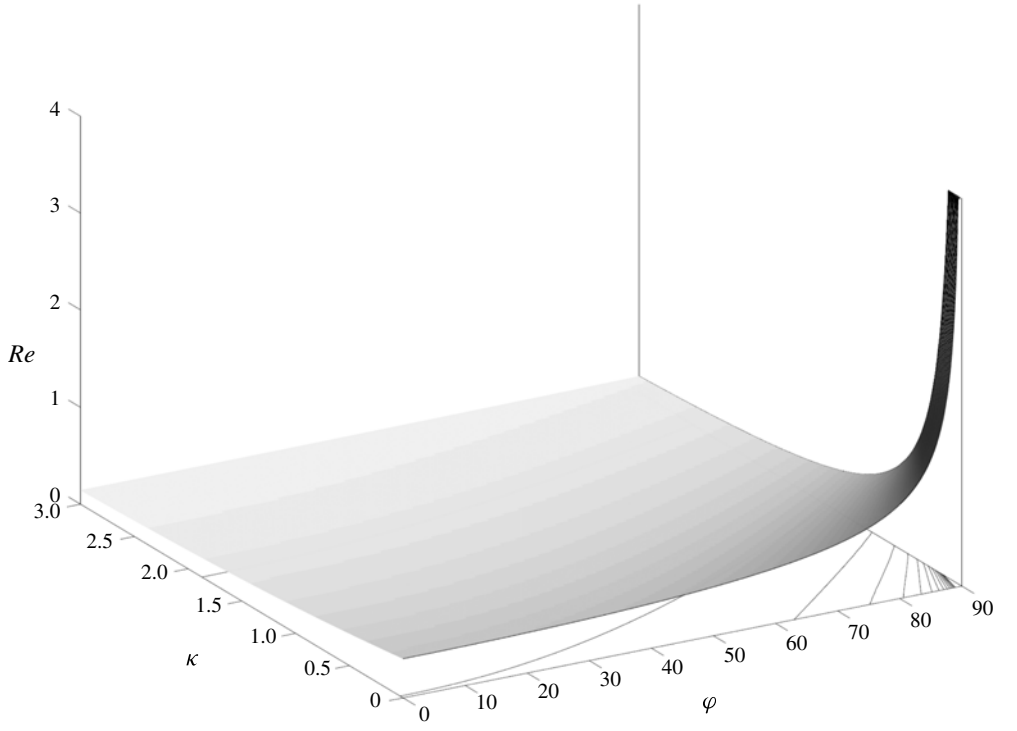

FIGURE 5. Surface plot and contour lines of the Reynolds number $Re = \bar{\theta}(\varphi, \kappa)$ as a function of the sweep angle φ and the wall suction κ, obtained by numerical integration of (2.15). The explicit dependence along the axis $\kappa = 0$ follows from (3.5*a*), and that along the axis $\varphi = \pi/2$ follows from (3.5*b*).

non-dimensional number φ relates all three parameters $\{W_\infty, \nu, a\}$ and therefore Re^{SH} must be a function of φ alone.

The same reasoning holds for the dependence of Re^{AS} on κ, because the ASBL does not have an extrinsic length scale.

A direct, explicit relation between Re and Re^{SH} is found by eliminating φ from (3.5*a*) and (3.6*a*) altogether:

$$Re|_{\kappa=0} = \frac{\bar{\theta}_0}{\sqrt{\cos\left[\operatorname{atan}(Re^{SH}/\bar{\theta}_0)\right]}} = \bar{\theta}_0 \left(1 + \left(\frac{Re^{SH}}{\bar{\theta}_0}\right)^2\right)^{1/4}. \tag{3.7}$$

If $Re^{SH} \gg 1$, which is usually the case in aerodynamics, this result may be further simplified to

$$Re|_{\kappa=0} \approx \sqrt{\bar{\theta}_0\, Re^{SH}}. \tag{3.8}$$

The transformation of $Re(\kappa)_{\varphi=\pi/2}$ to the classical, more familiar definition of the ASBL Reynolds number $Re^{AS}_{class} = W_\infty/V_0$ reads

$$Re(\kappa)|_{\varphi=\pi/2} = \frac{Q_l|_{\varphi=\pi/2}}{\sqrt{\nu\gamma|_{\varphi=\pi/2}}} = \frac{W_\infty\sqrt{\theta\left(\varphi=\dfrac{\pi}{2}\right)}}{\sqrt{\nu W_\infty}} = \frac{W_\infty\sqrt{\nu/(2V_0)}}{\sqrt{\nu W_\infty}} = \sqrt{\frac{Re^{AS}_{class}}{2}}, \tag{3.9}$$

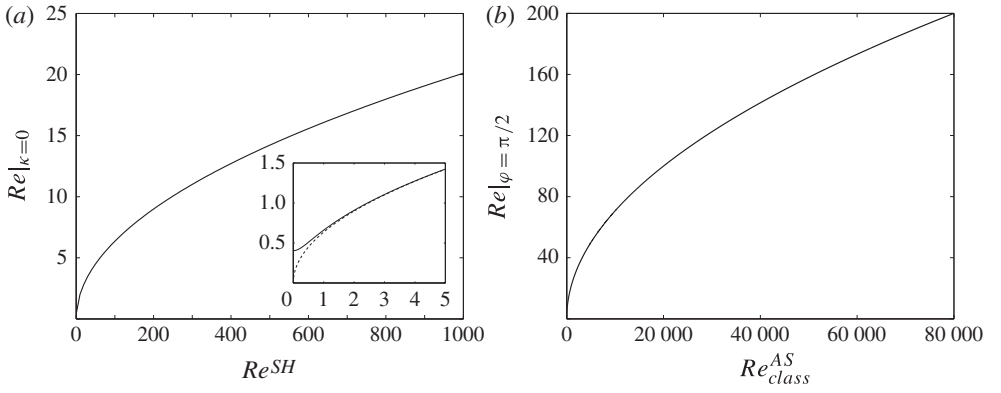

FIGURE 6. Dependence of Re on the classical Reynolds numbers Re^{SH} (as described by (3.7) and (3.8)) and Re^{AS}_{class} (as described by (3.9)). The dashed curve in the inset represents the asymptote (3.8).

where the second equality follows from (2.11) and the third from (3.5*b*). Relations (3.7), (3.5*b*) and (3.9) are illustrated in figure 6.

Finally, we highlight a duality. A unique pair (φ, κ) can be obtained not only by first calculating φ from the strain of a SHBL, using (3.6), upon which some suction κ^{SH} is then superimposed (transformed to κ); alternatively, κ may be computed first, based on an ASBL upon which far-field strain is then superimposed by letting the wall-normal velocity exceed the wall-suction velocity. The latter approach requires the definition of a non-dimensional 'strain number of the ASBL', say χ, from which φ may be calculated. With the condition that the strain number be zero in the absence of strain, it follows from dimensional analysis that

$$\chi := \frac{\sqrt{-\nu\,\mathrm{d}V/\mathrm{d}y}}{V_0} = \frac{\sqrt{\nu\gamma\cos\varphi}}{V_0} = \frac{\sqrt{\cos\varphi}}{\kappa} = \frac{1}{\kappa^{SH}}, \tag{3.10}$$

i.e. χ is the inverse of the classical parameter κ^{SH}. Therefore, the suction κ^{SH} of a SHBL may be interpreted as an inverse strain number of the corresponding ASBL, which determines by how much the ASBL is strained in the chordwise direction.

4. Linear stability theory

This section is devoted to linear stability analysis of the exact solutions given by (2.15). In § 4.1 the equations of linear stability of the SHBL with suction and those of the ASBL are derived. In contrast to the classical equations, the compound formalism (2.15) is used throughout. Common properties of the sets of equations are demonstrated analytically in § 4.2 before the compound linear stability problem is solved numerically in § 4.3. The compound formulation allows us to investigate the linear stability of the attachment-line boundary layer where the classical SHBL formulation becomes singular. This includes the cases where the leading-edge radius R^* tends to infinity or where the wing sweep angle Λ goes to 90°.

4.1. *Stability of the SHBL and the ASBL in compound formulation*

First, the stability partial differential equations (PDEs) for the two base flows are derived. Then, the compound formulation of the base flows and the classical modal

stability ansatz functions are substituted into these PDEs. This leads to two ODEs for the SHBL and two for the ASBL.

The velocity field is decomposed into a base flow $\boldsymbol{U}_B$ and disturbances $\boldsymbol{u}$ according to

$$\boldsymbol{U}(x, y, z, t) = \boldsymbol{U}_B(x, y) + \boldsymbol{u}(x, y, z, t). \tag{4.1}$$

All velocity components in this section are expressed in non-dimensional form

$$U_B(x, \eta) = \frac{\gamma\, x \Delta f'}{Q} = \frac{x f'}{Re}, \quad V_B(\eta) = \frac{-f}{Re}, \quad W_B(\eta) = g \sin\varphi, \tag{4.2a–c}$$

with $Re = Q/\sqrt{\gamma \nu}$ (cf. table 1).

4.1.1. *Linear stability equations of the SHBL*

Linearizing the NSE about the SHBL base flow $\boldsymbol{U}_B(x, y) = (U_B(x, y), V_B(y), W_B(y))^{\mathrm{T}}$ leads to the governing equations for the wall-normal disturbance velocity component v and the wall-normal disturbance vorticity $\zeta = (\boldsymbol{\nabla} \times \boldsymbol{u}) \cdot \boldsymbol{e}_y$:

$$\left[\left(\frac{\partial}{\partial t} + U_B\frac{\partial}{\partial x} + V_B\frac{\partial}{\partial y} + V_B' + W_B\frac{\partial}{\partial z}\right)\Delta + \left(-U_B''\frac{\partial}{\partial x} + V_B''\frac{\partial}{\partial y} - W_B''\frac{\partial}{\partial z}\right) + V_B''' + 2\frac{\partial U_B}{\partial x}\frac{\partial^2}{\partial x^2} - \frac{\Delta^2}{Re}\right] v = 2\left(\frac{\partial U_B'}{\partial x}\frac{\partial}{\partial x} + \frac{\partial U_B}{\partial x}\frac{\partial^2}{\partial x \partial y}\right) u, \tag{4.3a}$$

$$\left[\left(\frac{\partial}{\partial t} + U_B\frac{\partial}{\partial x} + \frac{\partial U_B}{\partial x} + V_B\frac{\partial}{\partial y} + W_B\frac{\partial}{\partial z}\right) - \frac{\Delta}{Re}\right]\zeta = \left[-U_B'\frac{\partial}{\partial z} + W_B'\frac{\partial}{\partial x}\right] v. \tag{4.3b}$$

This system of PDEs may be reduced to a system of ODEs by introducing the classical ansatz (Görtler 1955; Hämmerlin 1955)

$$\boldsymbol{u} = (\hat{u}(y) \cdot x, \hat{v}(y), \hat{w}(y))^{\mathrm{T}} \cdot \exp[\mathrm{i}(\beta z - \omega t)], \tag{4.4}$$

with $\beta \in \mathbb{R}$ and $\omega = \omega_r + \mathrm{i}\omega_i \in \mathbb{C}$. Together with (4.2), this leads to

$$[(\mathrm{i}\omega Re + f\mathcal{D} + f' - \mathrm{i}\beta Re\, g \sin\varphi)(\mathcal{D}^2 - \beta^2) + (f''\mathcal{D} + \mathrm{i}\beta Re\, g'' \sin\varphi + f''') + (\mathcal{D}^2 - \beta^2)^2]\hat{v} = -2(f'' + f'\mathcal{D})\hat{u}, \tag{4.5a}$$

$$[\mathrm{i}\omega Re - 2f' + f\mathcal{D} - \mathrm{i}\beta Re\, g \sin\varphi + (\mathcal{D}^2 - \beta^2)]\hat{u} = f''\hat{v}, \tag{4.5b}$$

subject to the homogeneous boundary conditions

$$\hat{u} = \hat{v} = \mathcal{D}\hat{v} = 0 \quad \text{for } y = 0, \infty. \tag{4.5c}$$

These classical linear stability equations are formally equivalent to (2.9*b*,*a*) of Hall *et al.* (1984), except for the factor $\sin\varphi$. The present definition of the Reynolds number Re differs greatly from that of Hall *et al.* (1984), who used Re^{SH} instead. The compound boundary layer formalism used here explicitly allows the chordwise base flow to vanish in the limit of $\varphi = 90°$.

4.1.2. *Linear stability equations of the ASBL*

Linearizing the NSE about the particular ASBL base flow $\boldsymbol{U}_B(y) = (0,\, V_B,\, W_B(y))^{\mathrm{T}}$ leads to

$$\left[\left(\frac{\partial}{\partial t} + V_B\frac{\partial}{\partial y} + W_B\frac{\partial}{\partial z}\right)\Delta - W_B''\frac{\partial}{\partial z} - \frac{\Delta^2}{Re}\right] v = 0, \tag{4.6a}$$

$$\left[\left(\frac{\partial}{\partial t} + V_B\frac{\partial}{\partial y} + W_B\frac{\partial}{\partial z}\right) - \frac{\Delta}{Re}\right] \zeta = -W_B'\frac{\partial v}{\partial x}. \tag{4.6b}$$

These equations are the same as those given by Fransson & Alfredsson (2003), but again with a different definition of Re. Using the usual normal-mode ansatz

$$\boldsymbol{u} = \left(\hat{u}(y),\ \hat{v}(y),\ \hat{w}(y)\right)^{\mathrm{T}} \cdot \exp[\mathrm{i}(\beta z + \sigma x - \omega t)] \tag{4.7}$$

and the compound boundary layer formalism (4.2), we obtain

$$\left[(\mathrm{i}\omega Re + \kappa\mathcal{D} - \mathrm{i}\beta Re\, g)(\mathcal{D}^2 - k^2) + \mathrm{i}\beta Re\, g'' + (\mathcal{D}^2 - k^2)^2\right]\hat{v} = 0, \tag{4.8a}$$

$$\left[\mathrm{i}\omega Re + \kappa\mathcal{D} - \mathrm{i}\beta Re\, g + (\mathcal{D}^2 - k^2)\right](\mathrm{i}\beta\hat{u} - \mathrm{i}\sigma\hat{w}) = \mathrm{i}\sigma Re\, g'\hat{v}, \tag{4.8b}$$

with $k^2 := \beta^2 + \sigma^2$, subject to the homogeneous boundary conditions (4.5*c*). Again, we have recovered the classical linear stability problem in the compound formulation, which explicitly takes into account the wall suction κ.

4.2. *Convergence of GH modes towards TS modes*

One of the principal results of the present work is that the three-dimensional linear GH mode of the SHBL with suction, given by (4.5), smoothly transforms into a two-dimensional TS mode of the ASBL, given by (4.8), as the angle of sweep φ of the flat plate goes to 90°. This finding is potentially of interest in view of the attachment-line instability, as the properties of the highly stable ASBL may be approached or even attained by increasing the sweep angle φ of the flat plate.

It is not straightforward to conclude this from § 2.2 alone. It was shown there that the base flow of the SHBL in the limit $\varphi = \pi/2$ is identical to the base flow of the ASBL. This does not automatically mean that the equations of linear stability, (4.5) and (4.8), become equal in that limit as well, given that they are based on two different ansatz functions (4.4) and (4.7). However, this can easily be verified by going to the limit $\varphi = \pi/2$, such that $f = \kappa$ and $f' = f'' = f''' = 0$ in the stability equations (4.5) of the SHBL. This leads to the same set of equations as would be obtained upon substituting $\sigma = 0$ into the ASBL stability equations (4.8). Thus, the stability equations (4.5) of the SHBL, which use the GH ansatz (4.4), are identical in the full-sweep limit to the modified Orr–Sommerfeld and Squire equations of the ASBL (4.8), derived under the ansatz (4.7), provided that $\sigma = 0$. In brief,

$$(4.5)|_{\varphi=\pi/2} \iff (4.8)|_{\sigma=0}. \tag{4.9}$$

Fortunately, the constraint that the chordwise wavenumber σ must vanish is of minor relevance, since the (unique) most unstable mode of the ASBL is the TS mode found for $\sigma = 0$.

The convergence of the GH modes towards TS modes in the full-sweep limit is interesting because the ansatz functions (4.4) of GH and (4.7) of TS modes are of

different polynomial orders in the x direction. While non-trivial solutions are found for $\hat{u}$, $\hat{v}$ and $\hat{w}$, as long as $\varphi < \pi/2$, only the two components $\hat{v}$ and $\hat{w}$ can be non-zero in the full-sweep limit. This is best seen by subtracting the continuity equation for the TS normal-mode ansatz (4.7) from the continuity equation for the GH ansatz (4.4). The trivial solution $\hat{u}|_{\sigma=0} \equiv 0$ overcomes the difference in polynomial order of the ansatz functions. This immediately raises the question of whether other arbitrary three-dimensional ansatz functions, e.g. GH-like functions, also converge towards $\hat{u}|_{\sigma=0} = 0$ and become TS waves in the full-sweep limit $\varphi = \pi/2$, such as the polynomial modes investigated by Theofilis *et al.* (2003) or the Hermite polynomials investigated by Obrist & Schmid (2003). It turns out that this is not the case, since the stability equations (4.3*a*) of the SHBL and (4.6*a*) of the ASBL become equal only when the terms containing second derivatives of v with respect to x vanish. Since these terms do not automatically tend to zero when taking the limit $\varphi = \pi/2$ ($U_B \equiv 0$, $V_B' \equiv 0$), they must be zero by construction for any GH-like ansatz, if the modes will become TS modes in the full-sweep limit. This reduces the chordwise x-dependence of unstable GH-like ansatz functions to polynomials of at most first order for v or at most second order for u. Other ansatz functions are not TS modes in the full-sweep limit.

4.3. *Numerical solution of the linear stability equations (4.5) for various φ and κ*

We numerically determine the neutral surface $\omega_i = 0$ of the stability equations (4.5) and thereby also confirm the theoretical results of the preceding subsection. The transformation of the wavenumber β and phase speed $c = \omega/\beta$ to β^{SH} and $c^{SH} = \omega^{SH}/\beta^{SH}$ of the SHBL and to β^{AS}_{class} and $c^{AS}_{class} = \omega^{AS}/\beta^{AS}$ of the ASBL read (cf. table 1)

$$\beta^{SH} = \beta/\sqrt{\cos\varphi}, \quad c^{SH} = c\sin\varphi, \tag{4.10a}$$

$$\beta^{AS}_{class} = \beta\sqrt{2Re^{AS}_{class}}, \quad c^{AS}_{class} = c. \tag{4.10b}$$

4.3.1. *Numerical solution method*

The solution of (4.5) requires the base flow (4.2), which is found by a shooting integration. The wall-normal extent of the computational domain is chosen as $L_y = 60 \cdot \bar{\theta}(\varphi, \kappa)$. The differential operator $\mathcal{D}$ is discretized with a Chebyshev spectral collocation method following Obrist & Schmid (2003), and the most unstable mode is found by an implicitly restarted Arnoldi method (Trefethen & Bau 1997). We search for neutral curves for $\kappa = \text{const.}$, starting from two manually obtained points on the lower branch and two points on the upper branch of each neutral curve. The neutral curves are extended by successive extrapolation of φ, β and c_r, followed by a Newton iteration to obtain exact values for which $|c_i| < 10^{-6}$. Since a good approximation to the real part c_r is found by extrapolation from known values, the Arnoldi iteration works robustly and converges very quickly throughout the entire $\{\varphi, \kappa, \beta\}$ parameter space investigated.

4.3.2. *The neutral surface*

The neutral surface in the parameter space $\{\varphi, \beta, \kappa\}$ is shown in figure 7(*a*). The results for the neutral curve on the plane $\kappa = 0$ (SHBL without suction) are almost in perfect agreement with those of Hall *et al.* (1984). The point corresponding to the critical Reynolds number Re^{SH}_{crit}, denoted by a filled square symbol, is at

$$\varphi_{crit}|_{\kappa=0} \approx 89.960\,286, \quad \beta_{crit} \approx 0.007\,58, \quad c_{r,crit} \approx 0.3825, \tag{4.11a–c}$$

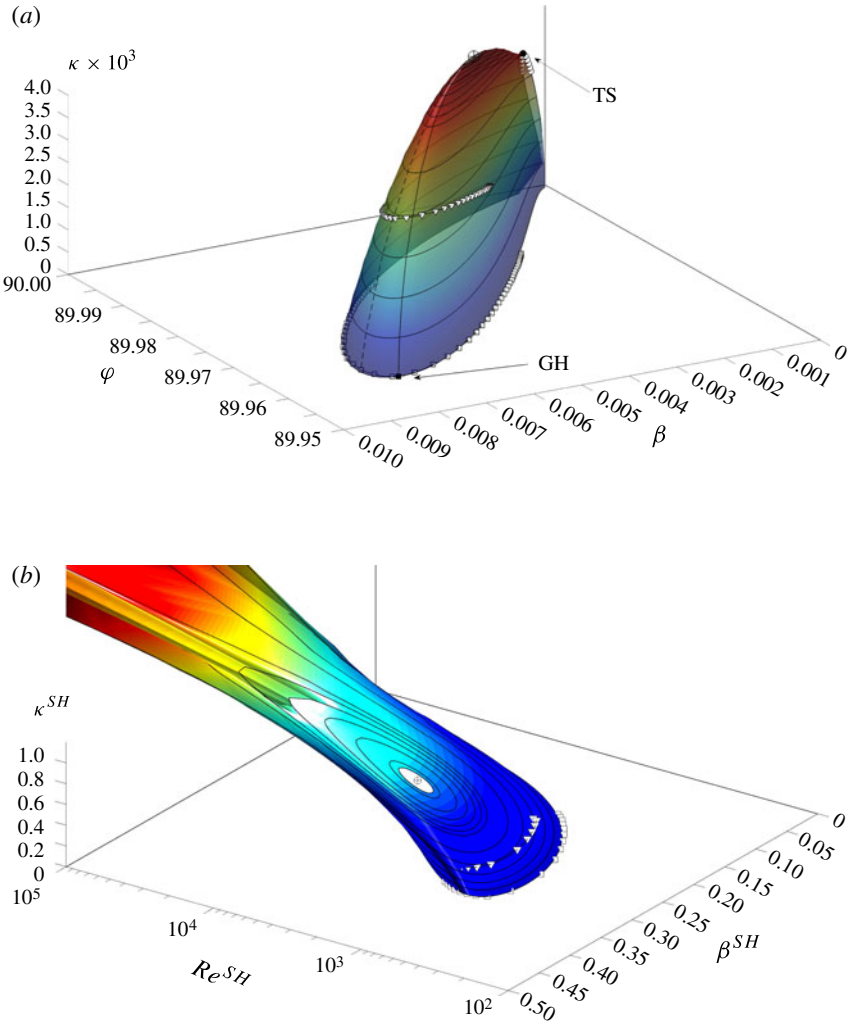

FIGURE 7. (Colour online) (*a*) Neutral surface of the eigenvalue problem (4.5) of the compound formalism (4.2) as a function of the sweep angle φ, boundary suction κ and disturbance wavenumber β. The two arrows indicate the classical GH solution without suction and the classical TS solution of the ASBL for the respective critical Reynolds numbers. Open symbols represent results of Hall *et al.* (1984) for $\kappa^{SH}=0$ ($\square$) and $\kappa^{SH}=0.1$ ($\triangledown$) and of Herron *et al.* (1985) ($\bigcirc$) for the ASBL. (*b*) The same neutral surface in the classical coordinate system $\{Re^{SH}, \beta^{SH}, \kappa^{SH}\}$; the stability results of the ASBL cannot be shown in this coordinate system.

$$Re^{SH}_{crit} \approx 583.1, \quad \beta^{SH}_{crit} \approx 0.288, \quad c^{SH}_{r,crit} \approx 0.3825. \tag{4.12a–c}$$

Of particular importance is the fact that the neutral surface remains bounded also for $\varphi = \pi/2$ (ASBL), except in the singular limit of $\kappa \to 0$. The neutral curve for $\varphi = \pi/2$ is in excellent agreement with the two-dimensional linear stability results for the ASBL reported by Herron *et al.* (1985). The point of strongest suction at which instability may occur corresponds to the classical critical Reynolds number $Re^{AS}_{class,crit}$.

It is denoted by a filled circle in figure 7(*a*) and is found at

$$\kappa_{crit}|_{\varphi=\pi/2} \approx 0.003\,024, \quad \beta_{crit} \approx 0.000\,4693, \quad c_{r,crit} \approx 0.150, \tag{4.13a–c}$$

$$Re^{AS}_{class,crit} \approx 54\,677, \quad \beta^{AS}_{class,crit} \approx 0.155, \quad c^{AS}_{r,class,crit} \approx 0.150. \tag{4.14a–c}$$

For nonzero values of the suction κ, we compare our results with those of Hall *et al.* (1984) for $\kappa^{SH} = 0.1$ and find that the neutral surface is in very good agreement. For ease of comparison, the neutral surface is illustrated again in figure 7(*b*) in the classical coordinate system $\{Re^{SH}, \beta^{SH}, \kappa^{SH}\}$ used by Hall *et al.* (1984). Here, an advantage of the compound boundary layer formalism becomes evident: figure 7(*a*) combines the linear stability results for the HBL, SHBL and ASBL on a single plot, whereas in figure 7(*b*) the neutral curve of the ASBL is projected to infinity ($Re^{SH} \to \infty$, $\beta^{SH} \to \infty$, $\kappa^{SH} \to \infty$).

In figure 7(*a*) a further curve (solid line) is shown, which is the locus of the critical suction $\kappa_{crit}(\varphi)$, i.e. the minimum suction κ required to obtain a neutrally stable flow for a given φ. For $\varphi \lessapprox 89.995°$, $\kappa_{crit}(\varphi)$ is increasing with φ. For $\varphi \gtrapprox 89.995°$, the critical suction $\kappa_{crit}(\varphi)$ decreases with φ, until the local minimum $\kappa_{crit} \approx 0.003\,024$ is reached at $\varphi = \pi/2$, which is the location of the TS mode of the ASBL. The dashed line indicates the largest wavenumbers $\beta(\kappa)$ for which unstable modes can be found. Two-dimensional projections obtained from figure 7 are displayed in figure 8. The global maximum of the neutral surface, represented by $\oplus$ in figures 7(*a*) and 8, occurs at

$$\hat{\kappa} := \max_{\omega_i=0} \kappa \approx 0.003\,5489, \quad \varphi_{\hat{\kappa}} \approx 89.995\,820, \quad \beta_{\hat{\kappa}} \approx 0.001\,9743. \tag{4.15a–c}$$

This maximum has the following physical interpretation: while in theory an ASBL may be kept stable at Reynolds numbers close to $Re^{AS}_{class} \approx 55\,000$, or $\kappa \approx 0.003$, already small deviations from the full sweep $\varphi = 90°$ may destabilize the flow (see figure 8*b*). Such deviations might be due to slight plate curvature (resulting in far-field strain $a > 0$) or a plate sweep angle different from exactly 90°. In order for the ASBL to remain linearly stable despite such imperfections, the suction must be as strong as $\hat{\kappa}$ in (4.15). According to (3.9) and (3.5*b*), this value may be converted to an ASBL Reynolds number,

$$Re^{AS}_{class,crit,min} := \min_{\Lambda} Re^{AS}_{class,crit} \approx 39\,700, \tag{4.16}$$

which can be understood as a lower robust stability limit. Below this value, any ASBL is linearly stable for all wavenumbers β at any far-field strain rate or sweep angle.

4.3.3. *Marginally stable eigenfunctions*

The GH or TS eigenfunctions along the solid curve in figure 7(*a*) are plotted in figure 9, where the y axis has been normalized by the boundary layer momentum thickness Re, as given in (3.3). The magnitudes of the real and imaginary parts have been scaled such that

$$\max_{y}(|\hat{u}|^2 + |\hat{v}|^2 + |\hat{w}|^2) = 1. \tag{4.17}$$

The eigenfunctions vary smoothly as one progresses along the curve in figure 7(*a*) for the SHBL without suction to the ASBL. The last mode is the two-dimensional TS wave, which emerges smoothly from the three-dimensional GH mode. As shown in § 4.2, the magnitude of the chordwise $\hat{u}$ component goes to zero smoothly when approaching the ASBL.

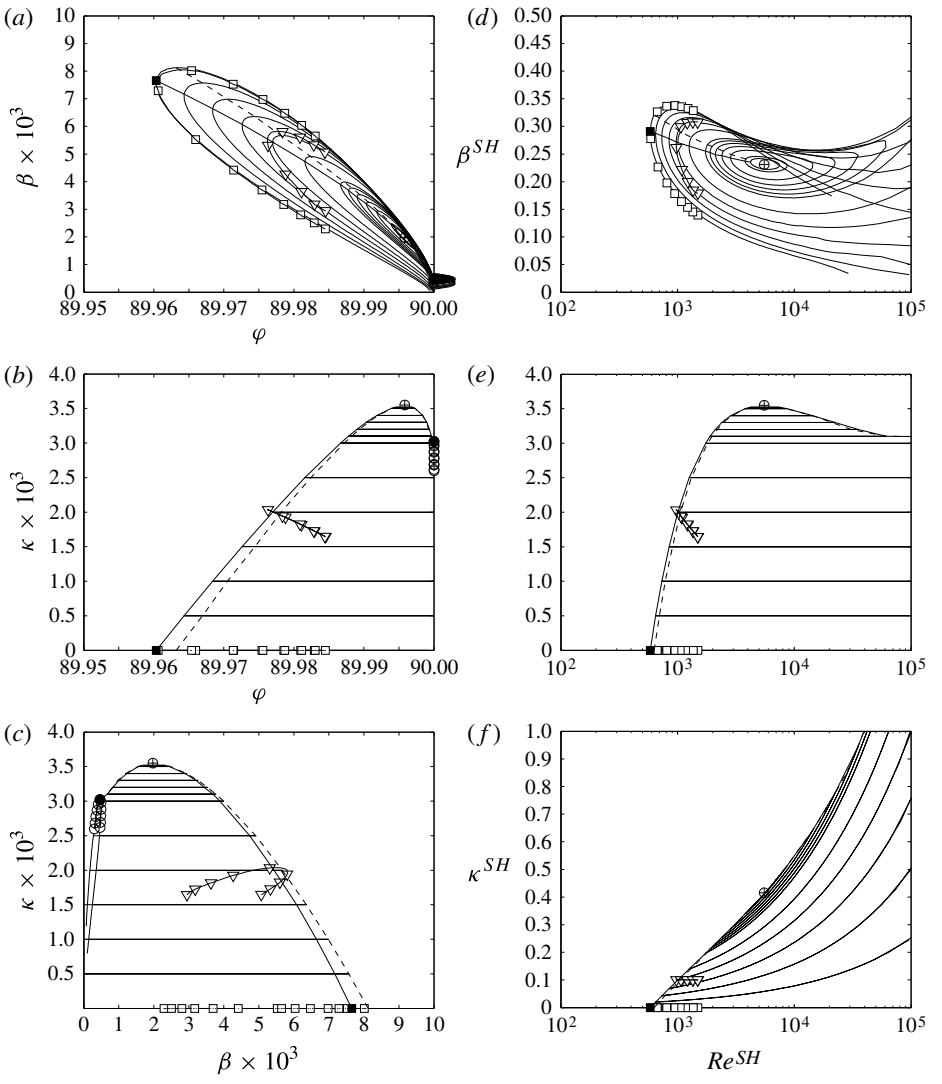

FIGURE 8. Projections of the neutral surface of figure 7 onto the various new (*a–c*) and classical (*d–f*) coordinates. In the new coordinate system, the region of linear instability and the neutral curve of the ASBL cover a finite area and are clearly visible in (*c*). This region cannot be shown when the classical coordinate system $()^{SH}$ of (*d*)–(*f*) is employed. In panels (*a*)–(*f*) the point of maximum suction κ is marked by the symbol $\oplus$. Open symbols denote results of Hall *et al.* (1984) for $\kappa^{SH} = 0$ ($\square$) and $\kappa^{SH} = 0.1$ ($\triangledown$) and of Herron *et al.* (1985) ($\bigcirc$) for the ASBL.

5. Conclusions

We have presented several boundary layer flows along a flat plate which had classically been regarded as unrelated and have reformulated them as a single, compound exact solution to the NSE (2.13). In particular, we have shown that the ASBL may be regarded as the flow found in a SHBL with suction in the limit of vanishing chordwise velocity. The classical SHBL formalism shows a singularity in

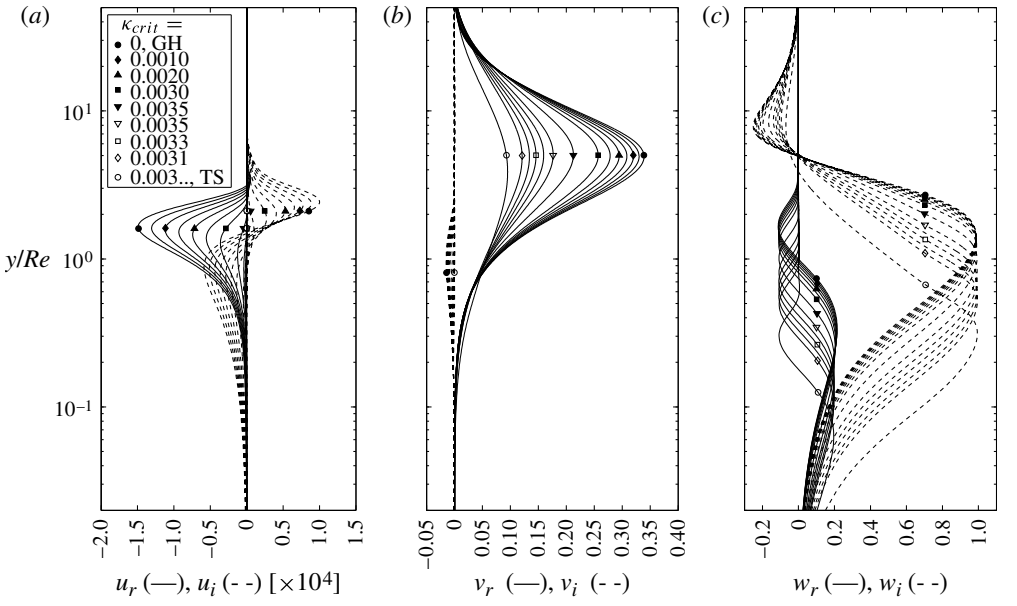

FIGURE 9. Neutral eigenfunctions along the locus κ_{crit}, depicted by a solid line in figure 7(*a*). Solid symbols denote eigenfunctions in the domain where $\partial\kappa_{crit}/\partial\varphi > 0$ and open symbols those for which $\partial\kappa_{crit}/\partial\varphi < 0$. The eigenfuctions are seen to vary smoothly from the GH mode in the SHBL without suction (•) to the TS mode of the ASBL (○).

that limit because the definition of the similarity coordinate η^{SH} is based only on the chordwise velocity component present in this flow, (2.1). This singularity has been overcome herein by introducing a new, compound similarity variable η, given in (2.12). The difference from the similarity variable used in known FS or FSC boundary layers lies in defining η simultaneously with respect to both the chordwise and sweep velocity components. This is realized through the introduction of a sweep angle φ as the new non-dimensional parameter (see figure 2), which leads to a different set of governing equations for the boundary layer flow. As a consequence of this new approach, the formalism in its most general form describes any flat-plate boundary layer flow with one homogeneous direction parallel to the plate (figure 3). This includes the SHBL, plane HBL, ASBL and OIBL (with non-zero angle of attack for the OIBL). The formalism also describes the swept OIBL, which serves as a model for the attachment-line flow subject both to an angle of attack and a sweep angle. Even further flows past a flat plate are contained as long as they are homogeneous (e.g. time-varying stagnation flow or stretching boundaries).

Owing to the redefinition of η, the classical non-dimensionalization could not be used. Rather, a new physical scaling (3.3) has been introduced, whose characteristic length scale is a function of the boundary layer momentum thickness. This quantity, and thus the Reynolds number Re, remains bounded in particular for both impingement flows without suction at the boundary and the ASBL without strain in the far-field (figure 5). Therefore, the new non-dimensionalization quantitatively describes the SHBL (with or without suction) and the ASBL, as well as the plane impingement boundary layer.

In the second part of this paper, a linear stability analysis of the new class of solutions has been carried out. This approach has unified the known results for the

classical SHBL and ASBL configurations. With this new, compound approach, the SHBL and ASBL have been shown to be connected through a common neutral surface (figure 7). In particular, it could be shown that the GH modes smoothly become TS modes when the parametric limit $\varphi = 90^\circ$ of the ASBL is approached (figure 9). The neutral surface has been reported for the entire parameter ranges of the sweep angle φ (0 to $\pi/2$) and the wall-suction κ (0 to very large), starting from the HBL without suction, moving along the SHBL without and with suction, and ending at the ASBL. Known classical results were confirmed where data were available (SHBL without suction and ASBL).

The combination of both the classical base flow solutions and analysis of their linear stability can be useful in gaining a better understanding of the attachment-line instability found on swept wings. First, it demonstrates how quantitatively similar the parallel-flow ASBL and the nearly parallel flow along the leading edge of wings are. Second, by adjusting the wing parameters (e.g. leading-edge radius, wing sweep angle) appropriately, the properties of the highly stable ASBL may be quantitatively recovered. In addition, the transformation presented herein from one classical base flow to another might allow extension of the nonlinear stability results known from the ASBL to the SHBL. An example of such concepts is the secondary streak-instability (Obrist *et al.* 2012) of the SHBL, which is stabilized by increasing suction (John, Obrist & Kleiser 2014).

Finally, a lower bound of approximately 39 700 for the classical ASBL Reynolds number has been found in (4.16), below which the ASBL remains linearly stable even if subject to an impingement flow component (e.g. due to plate curvature or a sweep angle).

Acknowledgements

We would like to thank F. Saggini for his contribution to the implementation of the Arnoldi eigenvalue solver. We acknowledge support of our work by the ETH research grant ETH-19 12-2.

REFERENCES

ARNAL, D., JUILLEN, J. C., RENEAUX, J. & GASPARIAN, G. 1997 Effect of wall suction on leading edge contamination. *Aerosp. Sci. Technol.* **1** (8), 505–517.

COOKE, J. C. 1950 The boundary layer of a class of infinite yawed cylinders. *Math. Proc. Camb. Phil. Soc.* **46** (04), 645–648.

DORREPAAL, J. M. 1986 An exact solution of the Navier–Stokes equation which describes non-orthogonal stagnation-point flow in two dimensions. *J. Fluid Mech.* **163**, 141–147.

DRAZIN, P. G. & RILEY, N. 2006 *The Navier–Stokes Equations: A Classification of Flows and Exact Solutions*. Cambridge University Press.

FRANSSON, J. H. M. & ALFREDSSON, P. H. 2003 On the disturbance growth in an asymptotic suction boundary layer. *J. Fluid Mech.* **482**, 51–90.

GASTER, M. 1967 On the flow along swept leading edges. *Aeronaut. Q.* **18**, 165–184.

GÖRTLER, H. 1955 Dreidimensionale instabilität der ebenen Staupunktströmung gegenüber wirbelartigen Störungen. In *50 Jahre Grenzschichtforschung. Eine Festschrift in Originalbeiträgen* (ed. H. Görtler & W. Tollmien), pp. 304–314. Vieweg.

HALL, P., MALIK, M. R. & POLL, D. I. A. 1984 On the stability of an infinite swept attachment line boundary layer. *Proc. R. Soc. Lond.* A **395** (1809), 229–245.

HÄMMERLIN, G. 1955 Zur Instabilitätstheorie der ebenen Staupunktströmung. In *50 Jahre Grenzschichtforschung. Eine Festschrift in Originalbeiträgen* (ed. H. Görtler & W. Tollmien), pp. 315–327. Vieweg.

HERRON, I. H., VON KERCZEK, C. H. & TOZZI, J. 1985 Instability characteristics of the asymptotic suction profile. *Trans. ASME J. Appl. Mech.* **52** (2), 487.

HIEMENZ, K. 1911 Die grenzschicht an einem in den gleichförmigen flüssigkeitsstrom eingetauchten geraden kreiszylinder. *Dingl. Polytech. J.* **326** (21–26), 321–324; 344–348; 357–362; 372–376; 391–393; 407–410.

HOCKING, L. M. 1975 Nonlinear instability of the asymptotic suction velocity profile. *Q. J. Mech. Appl. Maths* **28**, 341–353.

HOWARTH, L. 1951 The boundary layer in three-dimensional flow. Part 2. The flow near a stagnation point. *Phil. Mag.* **42** (335), 1433–1440.

JOHN, M. O., OBRIST, D. & KLEISER, L. 2012 An exact Navier–Stokes solution for three-dimensional, spanwise-homogeneous boundary layers. *Proc. Applied Maths Mech.* **12** (1), 477–478.

JOHN, M. O., OBRIST, D. & KLEISER, L. 2014 Stabilization of subcritical bypass transition in the leading-edge boundary layer by suction. *J. Turbul.* (to appear); doi: 10.1080/14685248.2014.933226.

KOLOMENSKIY, D. & MOFFATT, H. K. 2012 Similarity solutions for unsteady stagnation point flow. *J. Fluid Mech.* **711** (1), 394–410.

LEW, H. G. 1956 Asymptotic suction characteristics of the boundary layer over a circular cylinder. *J. Aeronaut. Sci.* **23** (9), 895–897.

LOK, Y. Y., AMIN, N. & POP, I. 2006 Non-orthogonal stagnation point flow towards a stretching sheet. *Intl J. Non-Linear Mech.* **41** (4), 622–627.

OBRIST, D., HENNIGER, R. & KLEISER, L. 2012 Subcritical spatial transition of swept Hiemenz flow. *Intl J. Heat Fluid Flow* **35**, 61–67.

OBRIST, D. & SCHMID, P. J. 2003 On the linear stability of swept attachment-line boundary layer flow. Part 1. Spectrum and asymptotic behaviour. *J. Fluid Mech.* **493**, 1–29.

OWEN, P. R. & RANDALL, D. G. 1952 Boundary layer transition on a sweptback wing. *Tech. Rep.* RAE-TM-AERO 277. Royal Aircraft Establishment, Farnborough.

PFENNINGER, W. 1965 Flow phenomena at the leading edge of swept wings. *Tech. Rep.* AGARDograph 97. North Atlantic Treaty Organization, Advisory Group for Aeronautical Research and Development.

POLL, D. I. A. 1979 Transition in the infinite swept attachment line boundary layer. *Aeronaut. Q.* **30**, 607–629.

PRESTON, J. H. 1948 The boundary-layer flow over a permeable surface through which suction is applied. *Tech. Rep.* RM 2244. Ministry of Supply, Aeronautical Research Council, London.

ROBITAILLIÉ-MONTANÉ, C. 2005 Une approche non-locale pour l'étude des instabilités linéaires: application à l'écoulement de couche limite compressible le long d'une ligne de partage. PhD thesis, Ecole Nationale Supérieure de l'Aéronautique et de l'Espace, Toulouse, France.

ROSENHEAD, L. 1963 *Laminar Boundary Layers*. Clarendon Press.

SARIC, W. S., REED, H. L. & WHITE, E. B. 2003 Stability and transition of three-dimensional boundary layers. *Annu. Rev. Fluid Mech.* **35**, 413–440.

SCHLICHTING, H. 1979 *Boundary-Layer Theory*, 7th edn. McGraw-Hill.

STUART, J. T. 1959 The viscous flow near a stagnation point when the external flow has uniform vorticity. *J. Aero. Sci.* **26** (2), 124–125.

TAMADA, K. 1979 Two-dimensional stagnation-point flow impinging obliquely on a plane wall. *J. Phys. Soc. Japan* **46** (1), 310–311.

THEOFILIS, V., FEDOROV, A. V., OBRIST, D. & DALLMANN, U. C. 2003 The extended Görtler–Hämmerlin model for linear instability of three-dimensional incompressible swept attachment-line boundary layer flow. *J. Fluid Mech.* **487**, 271–313.

TOOKE, R. M. & BLYTH, M. G. 2008 A note on oblique stagnation-point flow. *Phys. Fluids* **20** (3), 033101.

TREFETHEN, L. N. & BAU, D. 1997 *Numerical Linear Algebra*. Society for Industrial and Applied Mathematics.

WANG, C. Y. 1991 Exact solutions of the steady-state Navier–Stokes equations. *Annu. Rev. Fluid Mech.* **23**, 159–177.

WEIDMAN, P. D. 2012 Non-axisymmetric Homann stagnation-point flows. *J. Fluid Mech.* **702**, 460–469.